Arabian Journal of Chemistry (2021) **14**, 103096

King Saud University

Arabian Journal of Chemistry

www.ksu.edu.sa
www.sciencedirect.com

ORIGINAL ARTICLE

Biosynthesis of metallic nanoparticles from waste *Passiflora edulis* peels for their antibacterial effect and catalytic activity

T. My-Thao Nguyen [a], T. Anh-Thu Nguyen [a], N. Tuong-Van Pham [a], Quang-Vi Ly [a], T. Thuy-Quynh Tran [a], Thi-Dan Thach [a], Cam-Lai Nguyen [b], Kien-Sam Banh [c], Van-Dung Le [c,d], Linh-Phuong Nguyen [e], Dinh-Truong Nguyen [e], Chi-Hien Dang [c,d], Thanh-Danh Nguyen [c,d,*]

[a] *Tra Vinh University, Tra Vinh Province, Viet Nam*
[b] *Kien Giang Medical Colleges, Kien Giang Province, Viet Nam*
[c] *Institute of Chemical Technology, Vietnam Academy of Science and Technology, 1A, TL29 street, District 12, Ho Chi Minh City, Vietnam*
[d] *Graduate University of Science and Technology, Vietnam Academy of Science and Technology, 18 Hoang Quoc Viet, Cau Giay, Hanoi, Viet Nam*
[e] *School of Biotechnology, Tan Tao University, Long An Province, Viet Nam*

Received 5 January 2021; accepted 17 February 2021
Available online 24 February 2021

KEYWORDS

Passiflora edulis peel;
Nanoparticles;
Waste source;
Antibacterial;
Catalysis;
Waste water treatment

Abstract Recently, the waste agricultural materials have been widely considerable for green synthesis of noble metallic nanoparticles (MNPs) due to cost efficiency and environmental protection. This study has presented a simple method for the preparation of silver nanoparticles (AgNPs) and gold nanoparticles (AuNPs) utilizing aqueous extract of waste *Passiflora edulis* peel (PEP) as reducing and stabilizing agents. The formation of MNPs was optimized reaction conditions to obtain the best colloidal solutions. The characterizations of the biosynthesized MNPs were performed by analysis techniques such as Fourier transmission infrared spectroscopy (FTIR), X-ray diffraction (XRD), high-resolution transmission electron microscopy (HRTEM), selected area electron diffraction (SAED). The TEM data confirmed PEP-AgNPs and PEP-AuNPs in the spherical shape with mean size of 25 nm and 7 nm, respectively. The XRD and SAED patterns showed the synthesized nanoparticles existing in crystalline nature. Antibacterial and catalytic activities have been

* Corresponding author at: Institute of Chemical Technology, Vietnam Academy of Science and Technology, 1 Mac Dinh Chi Street, District 1, Ho Chi Minh City, Viet Nam.
E-mail addresses: ntdanh@ict.vast.vn, danh5463bd@yahoo.com (T.-D. Nguyen).
Peer review under responsibility of King Saud University.

Production and hosting by Elsevier

https://doi.org/10.1016/j.arabjc.2021.103096

investigated for their applications. The PEP-AgNPs exhibited a strong antibacterial activity against three strains including *Escherichia coli*, *Bacillus subtilis*, and *Staphylococcus aureus*. The excellently catalytic activity of both the biosynthesized nanoparticles has been demonstrated for reduction of nitrophenols and degradation of toxic organic dyes via study on their kinetics.

1. Introduction

Green chemistry using environmentally harmless materials as an alternative to fabrication of the chemical products has been particularly considerable in industry due to the world facing serious consequences to address pollution and low cost production [Chen et al., 2018; Ncube et al., 2020; Abdel-Shafy and Mansour, 2018]. The balance between economic growth and environmental protection is a principle challenge to create the sustainable industry. Eco-friendly and simple technique is an important solution that can achieve this aim through green chemistry [Zeng et al., 2011]. Challenges for chemists are to collect and convert knowledge of waste biological resource into compounds, process and method which need to achieve sustainable use and clean product [Ali et al., 2020; Lanzafame et al., 2017]. For this reason, green synthesis of the nanoparticles using waste resource have been sought to contribute to both aims in environmental protection and finding effective cost technique.

Nanoparticles are wide class of materials with dimensions < 100 nm which are applied in various fields such as pharmaceutical, environment, electronics and mechanical industries [Khan et al., 2019; Jeevanandam et al., 2018; Samyn et al., 2018]. Generally, various nanoparticles can be found as polymer nanoparticles [Zielinska et al., 2020], metallic nanoparticles (MNPs) [Shankar et al., 2016], ceramic nanoparticles [D. Singh et al., 2016], etc. Among them, the MNPs are widely considered due to their outstanding properties which can cause the development of different synthesis methodologies. Particularly, gold nanoparticles (AuNPs) and silver nanoparticles (AgNPs) biosynthesized from plant extracts are interested in various applications including antimicrobial agents [Talapko et al., 2020; Tang and Zheng, 2018], cancer agents [Rajeshkumar, 2016; Jain et al., 2012], catalysis [Astruc, 2020; Mitsudome and Kaneda, 2013] and sensors [Priyadarshini and Pradhan, 2017; Sabela et al., 2017]. The MNPs with nanometer sizes can easily penetrate cell walls and membranes of pathogenic microbes comparing to conventional antimicrobial drugs and effectively catalyze for organic reactions and environmental treatment. Comparing to the other synthetic methods, the MNPs synthesized via plant extract can reduce residual hazardous chemical species on the nanoparticle surface which is believed to be more biocompatible [Yadi et al., 2018]. Moreover, many plants possess intrinsic biomedical applications due to their stem contains the biologically active compositions including saponins, polyphenols, flavonoids, terpenoids and alkaloids.

Passiflora edulis is planted in many countries and its fruit is used widely as juice and pulp products for the food industry due to containing a good source of vitamin C [Goss et al., 2018]. The production process generates huge amounts of waste byproducts such as the peel that accounts about half of the fruit mass. According to studies on phytochemistry, *P. edulis* peel (PEP) contains insoluble and soluble pectin and polyphenol compounds such as carotenoids and flavonoids which contribute to its antioxidant capacity [Vuolo et al., 2019; Seixas et al., 2014]. On the other hands, these components play a role as the reducing and capping agents in preparation of MNPs, thus, its aqueous extract can be useful to effectively biosynthesize the MNPs. To the best of our knowledge, the PEP extract has not been used to reduce the metallic ions into MNPs so far. Here, we described green synthesis of AgNPs and AuNPs from aqueous extract of PEP and their applications as antibacterial agents and catalysts. This work made new contribution for green fields of technology applied for pharmaceutical chemistry and waste water treatment.

2. Experimental

2.1. Materials

Chemicals including $AgNO_3$, $HAuCl_4{\cdot}3H_2O$, $NaBH_4$, 2-nitrophenol (2-NP), 3-nitrophenol (3-NP), 4-nitrophenol (4-NP), methyl orange (MO), rhodamine B (RhB), rhodamine 6G (Rh6G) and eosin Y (EY) were purchased from Acros Company (Belgium). Waste *Passiflora edulis* fruit peels were collected at Tra Vinh city, Vietnam and dried in the air. The dried peels were grinded to obtain a fine powder. The powder (10 g) was refluxed with distilled water (100 mL) for 1 h and then the mixture was filtered. The filtrate was stored in the refrigerator (4 °C) for the further studies.

2.2. Optimization of nanoparticle biosynthesis

The biosynthesis was performed using the solution of $AgNO_3$ or $HAuCl_4$ and aqueous extract of PEP under continuous stirring at 1000 rpm in dark to avoid unnecessary photochemical reactions. Change in color of the mixture observed was inferred that the MNPs were successfully synthesized. The reaction mixture was stirred at different conditions including changes of metallic ion concentration (1.0–4.0 mM), volume ratios of metallic ion solution and extract (1:1 to 6:1, v/v), temperature (30–100 °C) and reaction time (200 min). The optimization of reaction conditions was explored via measurement of UV–Vis spectra in the range of 350–700 nm which can increase absorbance at the SPR peaks of around 420 nm for the biosynthesized AgNPs and 540 nm for the biosynthesized AuNPs. For the following studies, the MNPs were prepared in the optimized condition. The solid MNPs were obtained by centrifugation for 90 min at 6000 rpm and washed with the distilled water and then ethanol to remove the impurities. Finally, the MNPs were well dried in an oven at 60 °C.

2.3. Physicochemical characterization

Absorption spectra were carried out by measurement on UV–Vis spectrometer (1800 Shimazu, Japan). Fourier transform infrared (FT-IR, Tensor 27 FT-IR spectrophotometer, Bruker) was used to identify possibly functional groups of organic compounds presented in the extract and the nanoparticles. X-ray diffraction (XRD) patterns of crystal nanoparticles were measured on XRD-6100 X-Ray Diffractometer, Japan. TEM and HRTEM images and SAED pattern (JEOL JEM-1400) were utilized to analyze morphology and crystal structure of MNPs. Scanning electron microscope (SEM) images were obtained from S-4800 HI-9057–0006. Energy-dispersive X-ray (EDX) spectroscopy (EMAX ENERGY EX-400, Horiba) was used for chemical composition analysis. The zeta potential and particle size of the MNPs in aqueous solutions were determined by nanoPartica, Horiba SZ-100 (Japan). Thermogravimetry (TG) analysis was simultaneously measured on Discovery TGA 550 from 30 to 800 °C at a heating rate of 10 °C/min in the air atmosphere.

2.4. Antibacterial activity

The procedure for the antibacterial activity was carried out by the disk diffusion method. Three bacterial strains including *Escherichia coli* (Gram-negative) and *Bacillus subtilis*, *Staphylococcus aureus* (Gram-positive) were used to explore antibacterial activity of the biosynthesized AgNPs. Standard antibiotic ampicillin (0.01 mg/mL) and Luria–Bertani broth were used as positive and negative controls, respectively. Antibacterial activity was recorded using inhibition zone diameters (mm) around the paper disks. The PEP extract tested at volume of 10 μL exhibited no bioactivity with all bacterial strains.

2.5. Catalytic activity

The catalytic activity of PEP-AgNPs and PEP-AuNPs was evaluated by reduction of nitrophenols including 2-nitrophenol, 3-nitrophenol and 4-nitrophenol and degradation of dyes including MO, EY, Rh6G and RhB in the presence of excess $NaBH_4$ at the room temperature. Briefly, $NaBH_4$ solution (0.5 mL, 0.1 M) was added to pollutant solutions (2.5 mL, 0.1 mM) in a quartz cell. Then, PEP-AgNPs (25 μL) or PEP-AuNPs (25 μL) were added into the cell. The reduction was explored by using UV–Vis spectrophotometers in a scanning range of 300–800 nm. Gradual decrease in absorbance of 2-NP, 3-NP, 4-NP, MO, EY, Rh6G and RhB was observed at peaks of 414 nm, 383 nm, 400 nm, 464 nm, 515 nm, 525 nm and 554 nm, respectively. Reaction kinetics can be determined by measurement of UV–Vis spectra in a time-dependent manner. Because this work used a very low concentration of the pollutants with respect to the borohydride concentration and very low amount of MNPs (25 μL), the reaction kinetics could be considered as the pseudo-first-order reaction. The rate constant k could be determined by the equation $\ln (A_t/A_0) = -kt$, where t is the reaction time, $[A_0]$ is concentration of the pollutants at $t = 0$, and $[A_t]$ is concentration of the pollutants at time t. $[A_t]$ is determined from the absorbance values at maximum bands of the corresponding pollutants. The value k can be determined from slope of the linear line resulted by plotting $\ln(A_t/A_0)$ versus reaction time.

3. Results and discussion

3.1. Synthesis of biogenic nanoparticles

The study route of biogenic nanoparticles is illustrated in Fig. 1. The dried pieces of waste PEP were refluxed with water for 1 h before the extract was filtered in vacuum. The synthesis of nanoparticles was optimized for reaction conditions. The optimization was carried out by UV–Vis measurement to determine change absorption intensity of surface plasmon resonance (SPR) bands for AgNPs at 400–425 nm and AuNPs at 525–550 nm. To investigate stability of colloidal solutions, the optimized nanoparticles were stored at the ambient condition and changes in concentration of the synthesized nanoparticles were recognized by UV–Vis spectra. The optimized nanoparticles were physicochemically characterized by using analytic technologies and evaluating their antibacterial and catalytic activity including reduction of nitrophenols and degradation of toxic dyes.

The formation of stable colloidal solutions is strongly effected by reaction conditions which can be used to control size and morphology of the MNPs. In the present work, the reduction of metallic ions was explored in change of four principle parameters including metallic ion concentrations, ratios of extract volume to metallic ion solution volume, reaction temperature and reaction time. Based on SPR bands of relative MNPs, change of the nanoparticles concentration in colloidal solutions could be recognized by UV–Vis method which associated to change of absorption intensity.

The results are shown in Fig. 2. The effect of metallic ion concentrations on the formation of nanoparticles is clearly observed in Fig. 2A and 2E. At low concentrations (1.0–1.5 mM), the SPR bands of PEP-AgNPs were not appeared sharply, indicated no reduction of Ag^+ ions to AgNPs whereas a maximum value of absorption intensity was found at 1.5 mM of Au^{3+} ion. The absorbance of SPR band increased with concentrated silver ions and an optimum concentration was determined at 2.5 mM. The high concentrations induced decrease of absorption intensity which relates to the aggregation of the MNPs from colloidal solution.

The solutions of Ag^+ (2.5 mM) and Au^{3+} (1.5 mM) were used to study influence of volume ratios of metallic ion to extract in range of 1:1 to 6:1 (v/v). The results showed that the increase in the metallic ion volume induced an increase in concentration of the synthesized nanoparticles (Fig. 2B and 2F). For the biosynthesis of PEP-AgNPs, the SPR band was not appeared at the low ratios and only observed at 420 nm when volume ratios were over 3:1 (v/v). A maximum value of absorbance was achieved at a volume ratio of 5:1 (v/v). Meanwhile, the absorbance values of PEP-AuNPs at SPR wavelength (540 nm) was observed increasingly and achieved a maximum value at 3:1 (v/v). MNPs concentration in the colloidal solution reduced after the maximum value indicated that the amount of bioactive compounds is not enough for conversion of metallic ions into MNPs.

The investigation of reaction temperature was carried out in range of 30 – 100 °C. The results (Fig. 2C and G) showed that PEP-AgNPs were only formed after 60 °C and achieved an optimum value at 90 °C while the PEP-AuNPs were formed at low temperature (40 °C) and achieved an optimum temperature at 70 °C. The higher temperatures induced an aggrega-

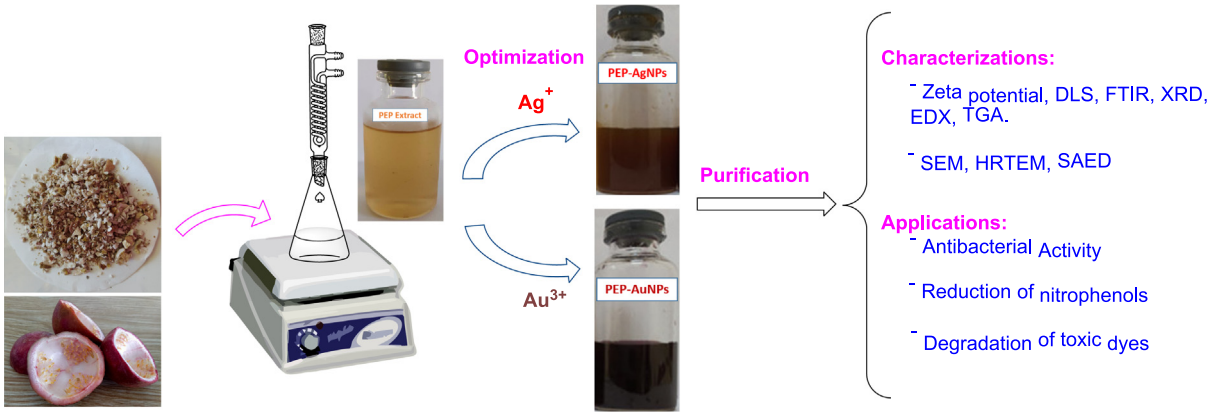

Fig. 1 Schematic illustration for synthesis and application of PEP-AgNPs and PEP-AuNPs biosynthesized by aqueous extract of waste *Passiflora edulis* fruit peel.

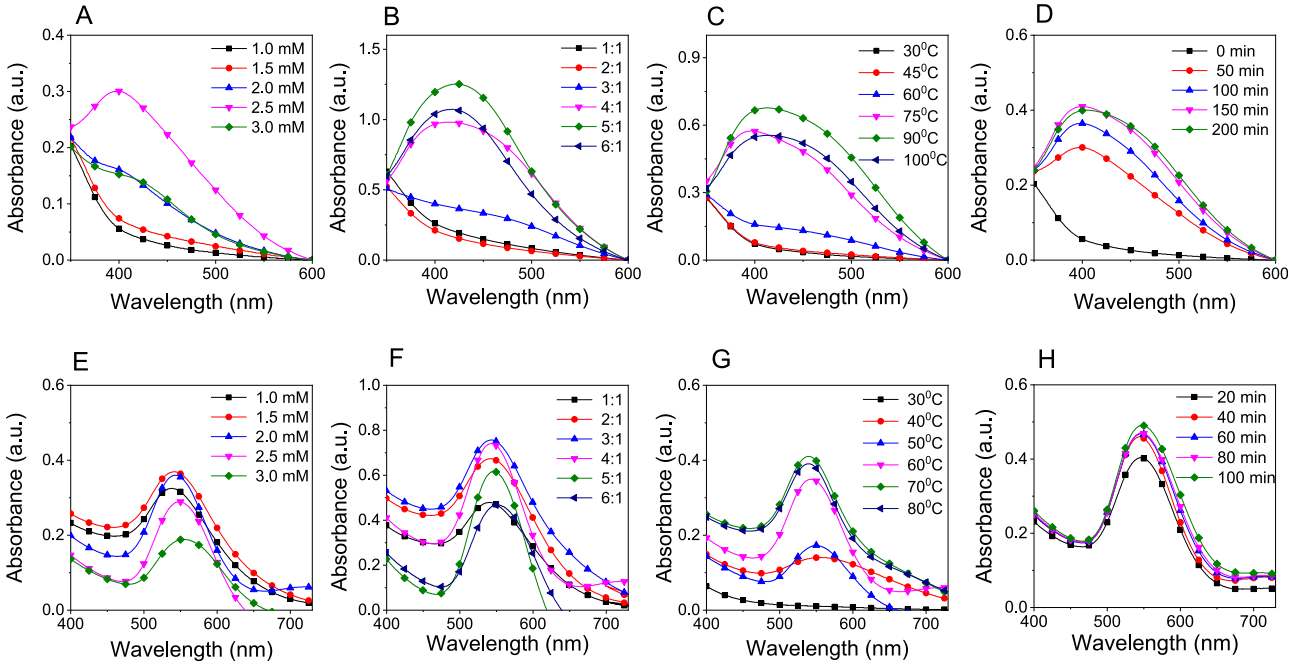

Fig. 2 UV–vis spectra for optimization of biosynthesis conditions including metallic ion concentrations, volume ratios of metallic ion solution to extract, reaction temperature and reaction time of PEP-AgNPs (A, B, C, D) and PEP-AuNPs (E, F, G, H).

tion of MNPs solid from colloidal solutions which were confirmed by decrease of absorption intensity in UV–Vis spectra. The observation revealed that the yield of MNPs biosynthesis strongly depends on reaction temperature.

The effect of reaction time for the biosynthesis of MNPs can be observed clearly in Fig. 2D and 2H. Increase of the absorbance values at the SPR bands confirmed higher MNPs concentration in the colloidal solution with longer reaction time. Results of PEP-AgNPs synthesis showed that the concentration of AgNPs was achieved over 60% when the solutions stirred in initial 50 min and the reduction was completed after 150 min. Meanwhile, the formation of AuNPs occurred faster and achieved over 80% after only initial 20 min. The concentration of formed nanoparticles was almost insignificantly increasing after 40 min. Moreover, there was no change in SPR bands for all investigated parameters confirmed the size and morphology of AgNPs insignificantly changed.

The results indicate that the reduction of Au^{3+} ions is much easier than reduction of Ag^{+} ion. It can be due to the reduction potential of Au^{3+}/Au (+1.5 V) more than that of Ag^{+}/Ag (+0.8 V) [Lide 2006]. For further study on their physicochemical properties and applications, the optimized PEP-AgNPs and PEP-AuNPs samples were prepared at 2.5 mM, 5:1 (v/v), 90 °C, 150 min and 1.5 mM, 3:1 (v/v), 70 °C, 40 min, respectively.

3.2. Characterization

Infrared spectroscopy analysis was carried out to determine possibly functional groups presented in PEP extract and the

biogenic nanoparticles as illustrated in Fig. 3. The FTIR data of the synthesized nanoparticles exhibited absorption bands similarly to that of the aqueous extract. It confirms the bioactive compounds as the stabilizing agent presented in the biogenic nanoparticles. The PEP extract spectrum appeared major bands including 3551, 2929, 1750, 1619, 1234 and 1182 cm^{-1}. These bands shifted to new positions in the spectra of MNPs indicated that bioactive components in the PEP extract including flavonoids, glucosides and proteins reduced metallic ions into MNPs. FTIR data of the biogenic nanoparticles showed the bands at 3423, 2921, 1616 and 1230 cm^{-1} for PEP-AgNPs and at 3461, 1636, 1249, 1052 cm^{-1} for PEP-AuNPs. The bands of 3400–3500 cm^{-1} presented in all the samples were attributed to OH stretching vibrations of glucoside compounds. The bands at 2929–2921 cm^{-1} were corresponded to —CH_2 stretching of polysaccharides [Keijok et al., 2019]. The bands at 1750–1620 cm^{-1} were assigned for C═O and C—N stretching confirming the presence of proteins in the PEP extract [Jyoti and Singh, 2016]. The shift of these bands observed in the spectra of biogenic nanoparticles indicates MNPs binding to the protein chains.

For study on stabilization of the formed nanoparticles, the colloidal solutions were utilized to measure zeta potential and dynamic light scattering (DLS) distribution at 25 °C. The content of elemental compositions presented in solid samples was determined by energy dispersive X-ray (EDX) analysis. The results are shown in Fig. 4. The colloidal solution of PEP-AgNPs and PEP-AuNPs possessed high negative zeta potentials of −34 mV and −46 mV, respectively which confirmed the highly stable nanoparticles solution. The size distribution profiles (Fig. 4B and E) showed that the PEP-AgNPs size was observed in a broad range of 30–5000 nm with a mean size of 310 nm (PI = 0.9) and the PEP-AuNPs size was found in a broad range of 3–5000 nm with a lower mean size of 104 nm (PI = 0.7). It reveals that the synthesized nanoparticles possess polydisperse distributions and can exist aggregation of the nanoparticles in colloidal solutions during synthetic process.

EDX analysis of solid PEP-AgNPs showed a strong peak at 3.0 keV that confirms the presence of silver element in the sample. Particularly, the presence of chloride element at 2.6 keV reveals the aqueous extract possessing a high content of chloride which can precipitate with silver ions during the synthetic process. The average content of silver element is estimated to be 81.53% (w/w) while the average content of gold elements is found from EDX pattern of PEP-AuNPs to be 83.50% (w/w). The high content of silver and gold in samples can allow to be applied as the effectively heterogeneous catalysts.

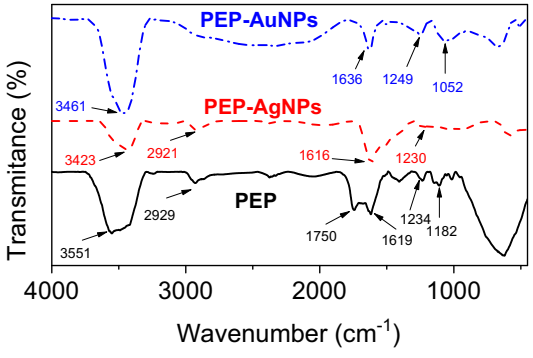

Fig. 3 FT-IR spectra of PEP extract, PEP-AgNPs and PEP-AuNPs.

The crystalline structure of MNPs is characterized by XRD analysis as illustrated in Fig. 5. The XRD pattern of PEP-AgNPs showed characteristic peaks of crystalline Ag (0) at 2θ angles of 38.15° (111), 64.52° (220) and 77.46° (311) (card number 00-004-0783) [Doan et al., 2020a]. The pattern also showed the strong peaks at 2θ angles of 27.83° (111), 32.54° (200), 46.30° (220), 54.79° (311), 57.52° (222) and 68.0° (311) that are typical for the face-centered cubic (fcc) structure of crystalline AgCl. The XRD data confirms the formation of AgCl crystal produced from reaction of silver ion with chloride ion presented in aqueous extract of PEP [Doan et al., 2020b]. The typical peaks of the face-centered cubic structure for crystalline Au (0) were assigned at 2θ angles of 38.25° (111), 44.45° (200), 64.67° (220), and 77.53° (311) (card number 00-004-0784). The results confirm successful biosynthesis of the crystalline metallic nanoparticles from PEP extract.

To investigate thermal behavior of the synthesized nanoparticles, thermogravimetric analysis (TGA) were carried out in the air atmosphere at a heating rate of 10 °C min^{-1} in air flow of 20 mL min^{-1}. The solids including PEP extract, PEP-AgNPs and PEP-AuNPs were used for the measurement. The results showed different thermal behaviors between the samples. The high stability of the biogenic nanoparticles compared to the PEP extract is observed in Fig. 6. The PEP extract shows decomposition at temperature region below 100 °C which is attributed to the evaporation of water and volatile compounds. The extract sample lost rapidly about 50% weight in temperature region below 300 °C while only 30% weight was lost in high temperature region (300–800 °C). The ash remained after heat process can be related to inorganic salts (e.g. Cl^-) in the PEP extract. Both the nanoparticles samples with the high stability in low temperature region (below 250 °C) indicated that the samples did not adsorbed water during storage process. The curve of PEP-AgNPs showed weight loss in region 270–350 °C and there is almost no weight loss in higher temperature region. The thermal stability of PEP-AuNPs is slightly lower than that of PEP-AgNPs. The weight loss of both nanomaterial samples in high temperature region can be related to oxidation of organic compounds stabilizing nanoparticles. Total weight loss of PEP-AuNPs is estimated about 27% in temperature region of 250–700 °C. The result reveals that the amount of organic compounds around the PEP-AgNPs is higher than that of PEP-AuNPs.

The surface morphology and size of the synthesized nanoparticles were investigated by SEM and HR-TEM techniques. The SEM microscopy was carried out on the dried samples after the centrifugation process while the TEM and HR-TEM measurements were applied for drops dried on the gold substrate. The results are shown in Figs. 7 and 8. SEM images showed that both the nanoparticles existed to be spherical in shape and uniform in size and the nanoparticles were agglomerated in the clusters by the centrifugation at high speed (Fig. 7A and 8A). The particle size of AgNPs (around 50 nm) is observed to be much greater than the size of AuNPs (around 20 nm).

As seen in Fig. 7B and 8B, The PEP-AgNPs and PEP-AuNPs are almost formed in uniform spheres dispersing well in colloidal solution. Supported to SEM results, TEM images showed that size of PEP-AgNPs is much higher than that of PEP-AuNPs. The size of AgNPs is distributed in range of 3–

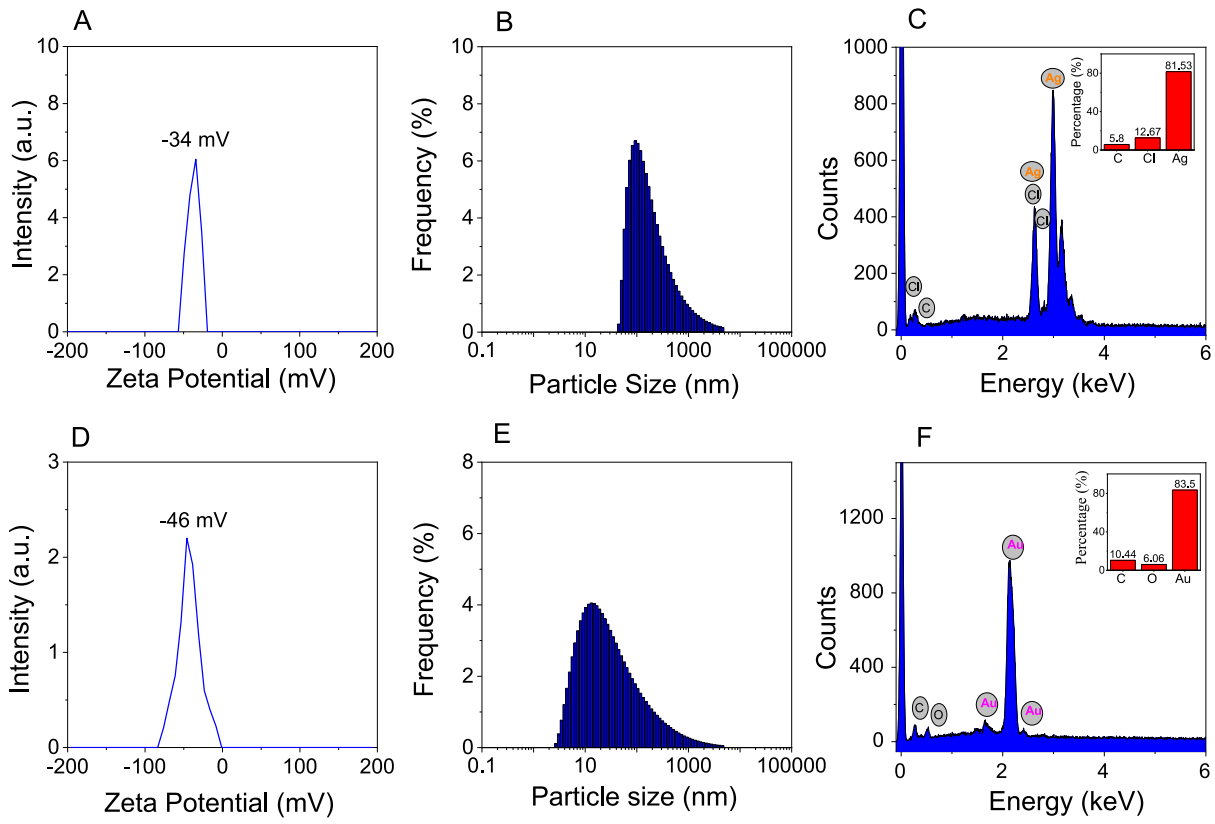

Fig. 4 Zeta Potential, Dynamic light scattering, energy dispersive X-ray analysis of PEP-AgNPs (A, B, C) and PEP-AuNPs (D, E, F).

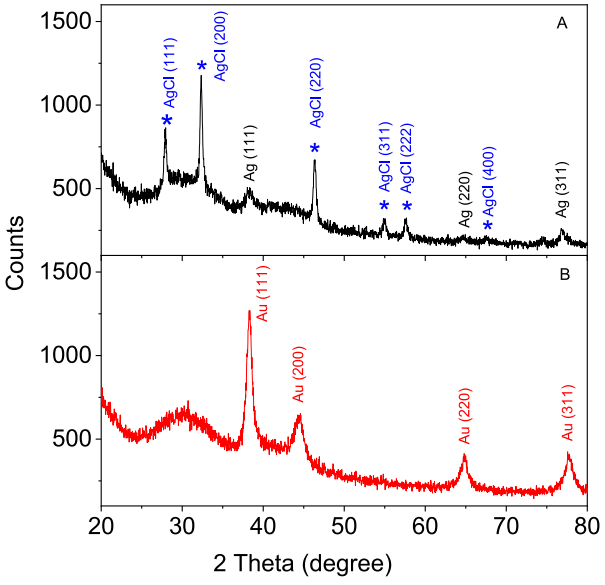

Fig. 5 XRD patterns of biosynthesized PEP-AgNPs and PEP-AuNPs.

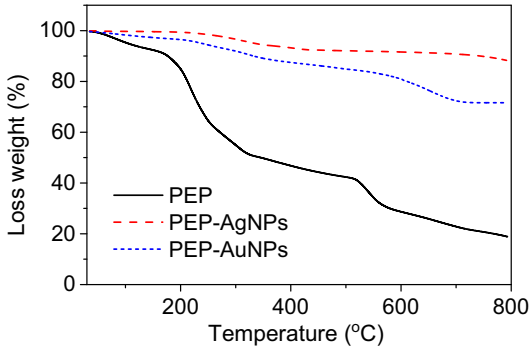

Fig. 6 TGA curves of PEP extract, PEP-AgNPs and PEP-AuNPs at heating rate of 10 °C min^{-1} in air flow of 20 mL min^{-1}.

35 nm with mean size of 25 nm while distribution of AuNPs ranges from 1 to 15 nm with mean size of 7 nm.

The crystalline nature of both biogenic nanoparticles can be clearly observed by HR-TEM and SEAD images (Fig. 7C, D, 8C and D). The lattice fringe of PEP-AgNPs and PEP-AuNPs corresponding to the fcc plane (111) possessed *d*-spacing of 0.20 and 0.21 nm, respectively. For selected area of electron diffraction (SAED) patterns, based on the interplanar distances, bright rings in both the nanoparticles confirmed the presence of crystalline nature, in agreement with XRD data. The presence of both crystalline Ag and AgCl can be observed in sample of PEP-AgNPs. The rings are related to fcc planes of the crystalline lattice of AgCl (111), (200), (400), (220), (222), and (311) and Ag (111), Ag (200) [Maldonado-Muñiz et al., 2020]. The crystalline lattice of AuNPs relates to fcc planes of (111), (200), (220) and (311) [P. Singh et al., 2016].

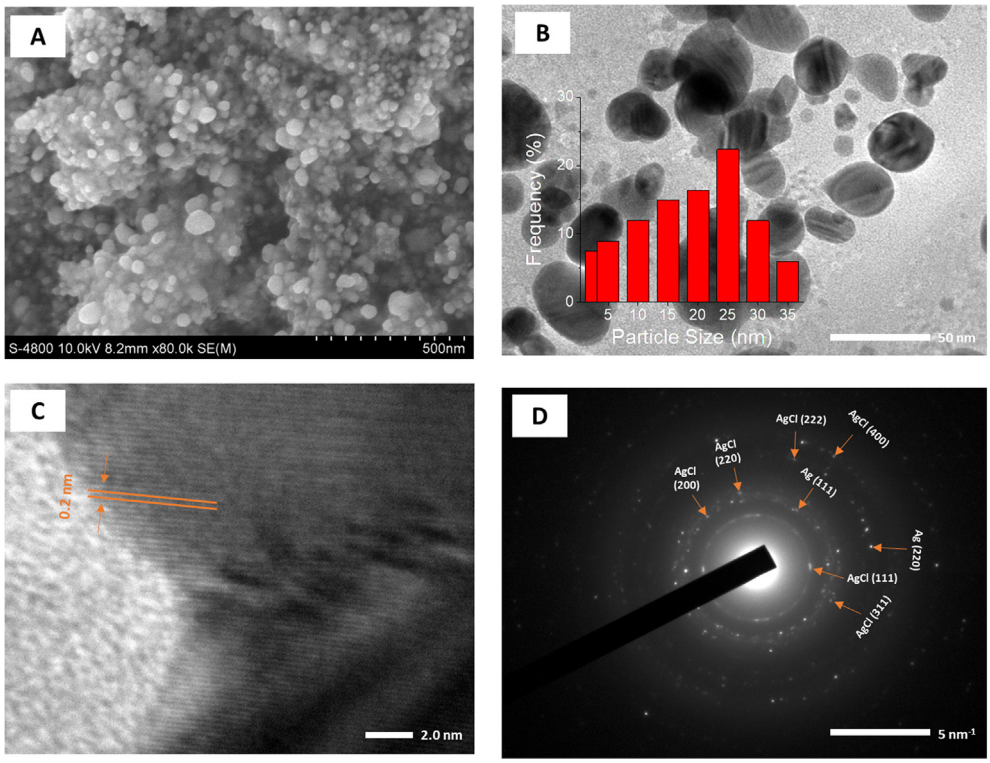

Fig. 7 SEM image (A); TEM image (B) and size distribution (inset); HRTEM image (C) and SAED pattern (D) of PEP-AgNPs.

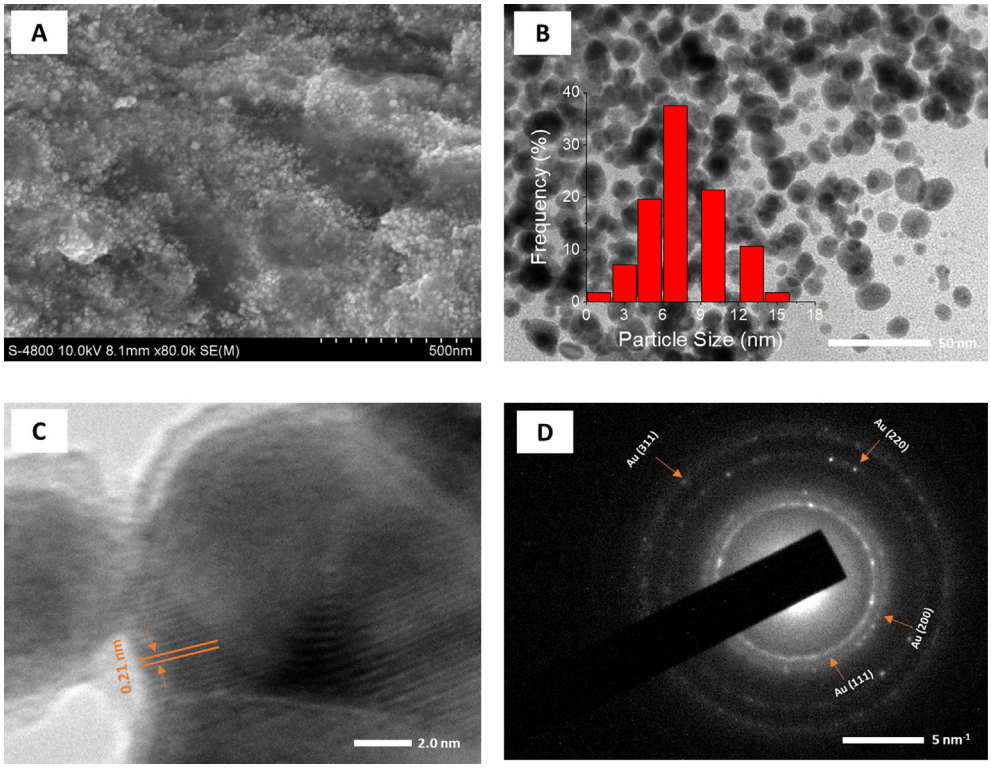

Fig. 8 SEM image (A); TEM image (B) and size distribution (inset); HRTEM image (C) and SAED pattern (D) of PEP-AuNPs.

3.3. Stability

Because the high PI value obtained from the DLS analysis recorded the agglomeration of the biosynthesized nanoparticles, their stability in the colloidal solution which strongly influenced on the chemical properties and applications, should be investigated during the storage process. In this work, the optimum MNPs solutions were exposed to daylight at room temperature and the concentration of nanoparticles were investigated by UV–Vis spectroscopy measurement after 4, 8, 12, 20, 28 days. Consequently, the stability can be determined by decrease of the absorbance at respective SPR bands. As seen in Fig. 9, both the nanoparticles are stable in initial 4 days which can be confirmed by no change of absorbance values. For PEP-AgNPs, rapid decrease in the nanoparticles concentrations is observed over time. AgNPs are lost about 32% after 8 days and 47% after 12 days, however, this stability maintains until 28 days of the exposition. PEP-AuNPs lost only 11% after 8 days and 17% after 28 days of the exposition. It is clear that PEP-AgNPs are more unstable than PEP-AuNPs that are supported by the previous DLS data. Notably, the MNPs synthesized from the PEP extract exhibit higher stability in comparison with the other plants e.g. waste *Nypa fruticans* fruit husk [Doan et al., 2020b], *Ocimum Sanctum* leaves [Jain and Mehata, 2017].

3.4. Antibacterial activity

For evaluation of the bioactivity, the MNPs and extract have been tested against three bacterial strains including *E. coli, B. subtilis* and *S. aureus* at the various concentrations. The Luria–Bertani broth and ampicillin were used as negative and positive controls, respectively. PEP extract (10 µL) and PEP-AuNPs at the highest concentration exhibited no effect against all tested bacterial strains. This observation is similar to the previous reports on the other plants [T.T.N. Nguyen et al., 2018; Vo et al., 2019]. The inhibition of PEP-AgNPs against the bacteria with various concentrations is presented in Fig. 10. The result shows that the antibacterial activity is increasing with concentrated nanoparticles and minimum inhibition concentration (MIC) values are found to be 1.0 mM for all the strains. Additionally, its bioactivity is slightly different among the tested strains that correlates to antibacterial mechanism depending on the cell wall and membrane generation through hydrophobic and bioaccumulation mechanism [Ahmad et al., 2020, Khameneh et al., 2019].

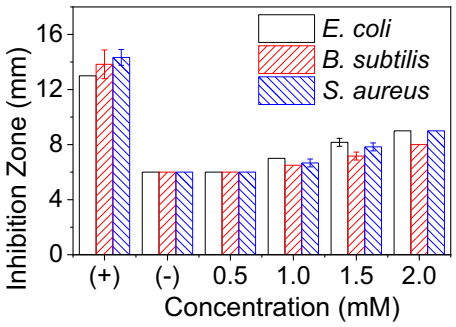

Fig. 10 Plot zone of inhibition (mm) for the varied concentrations of PEP-AgNPs inhibiting three different bacterial strains. Positive control using a standard antibiotic ampicillin (0.01 mg/mL); negative control using Luria–Bertani broth.

3.5. Catalytic activity

Catalytic reduction of toxic organic compounds including nitrophenols and organic dyes has been paying considerable attention in environmental field and organic chemistry. Due to their high stability in the normal condition, these compounds pose serious threat to the life environment [Ismail et al., 2019, Cíntia et al., 2019]. Indeed, the present work has utilized the biogenic MNPs as the heterogeneous catalysts for reduction of nitrophenols and degradation of toxic organic dyes by $NaBH_4$ as a hydrogenation reagent. The reaction kinetics are also investigated to make an insight into the catalytic behavior of the nanoparticles.

Reduction of nitrophenols

Conversion of nitrophenols into aminophenol derivatives has great potential in pharmaceutical applications because many of aminophenol products are principle materials and precursors for numerous drugs such as sulfonamide drugs (e.g. prontosil, sulfanilamide, ect.) [Capasso and Supuran, 2014], pain treatment drugs (e.g. paracetamol, phenacetin) [Clissold, 1986]. The reduction of nitrophenols in the presence of $NaBH_4$ without catalyst is well known as the thermodynamically favorable reaction. However, the kinetic barrier of adding the BH_4^- ion into nitrophenols induced a kinetically unfavorable reaction. Thus, the metal catalysts can be used as an electron transfer reagent to overcome this kinetic barrier. In this

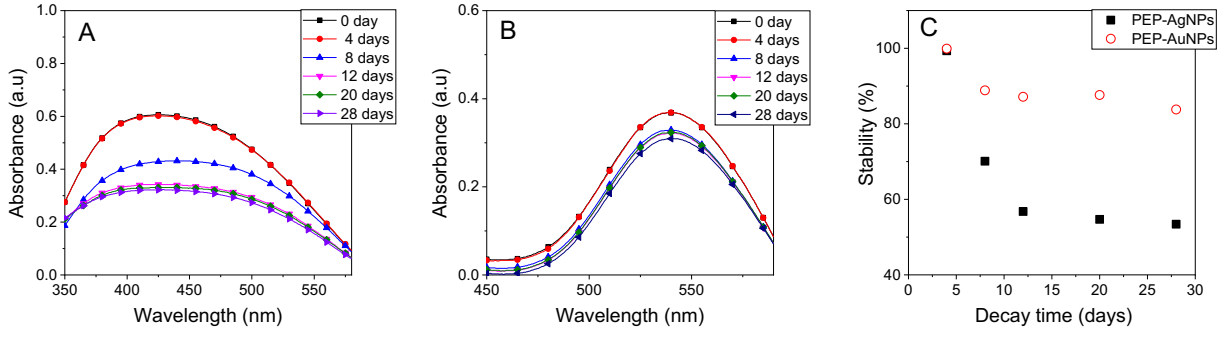

Fig. 9 UV–Vis spectra of PEP-AgNPs (A) and PEP-AuNPs (B) and plot of stability *vs* time (C) stored in daylight and room temperature.

work, we have investigated reduction of three different nitrophenols including 2-NP, 3-NP and 4-NP in the presence of PEP-AgNPs and PEP-AuNPs as heterogeneous catalysts in water medium. The kinetic investigation of the reaction was *in situ* monitored via directly recording UV–Vis spectra from the cuvette. The results are shown in Fig. 11. The color of nitrophenols is changed upon the addition of $NaBH_4$ confirmed the formation of phenolate ions and the UV–Vis spectra appear respective maximum peaks. The results showed their activity depending on the used substrates. The conversion of 2-NP and 4-NP into corresponding amine derivatives occurs over 20 min for both the catalysts, much slower than that of 3-NP (only 8 min for PEP-AgNPs and 12 min for PEP-AuNPs). The various values of kinetic constant can be found for reduction in the presence of two the catalysts. PEP-AgNPs catalyst found the rate constants of 2-, 3- and 4-nitrophenols being 1.15×10^{-3} s^{-1}, 2.45×10^{-3} s^{-1} and 1.58×10^{-3} s^{-1}, respectively while these values found for PEP-AuNPs catalyst to be 1.39×10^{-3} s^{-1}, 0.67×10^{-3} s^{-1} and 1.32×10^{-3} s^{-1}, respectively. In general, the kinetic investigation showed that the PEP-AgNPs catalyst exhibited slightly higher catalytic activity in comparison with the PEP-AuNPs synthesized in the optimum condition. Moreover, MNPs biosynthesized from PEP extract show higher catalytic efficiency than the relative MNPs synthesized from other plants that is listed in Table 1.

In addition to kinetic rate constants, turnover number (TON) and the turnover frequency (TOF) parameters are important to evaluate the catalytic activity of the heterogeneous catalysts. TON is identified as the number of substrate moles that 1 mol of the catalyst can convert substrates into products while TOF is calculated simply by TON/reaction time. TOF values of PEP-AgNPs for reduction of 2-, 3- and

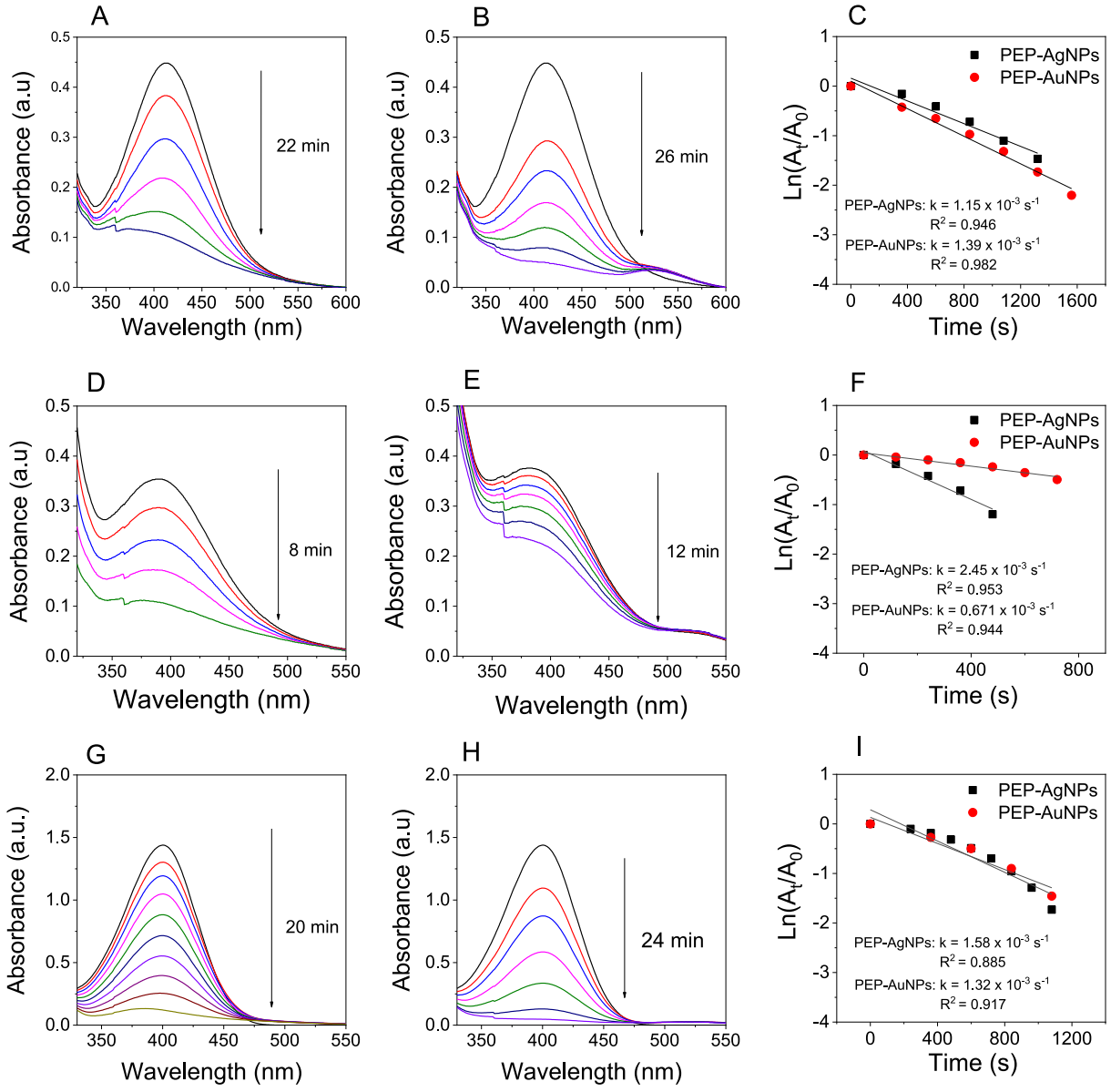

Fig. 11 UV–vis spectra in the presence of PEP-AgNPs (left), UV–vis spectra in the presence of PEP-AuNPs (middle), first order kinetics (right) for reduction of 2-nitrophenol (A, B, C), 3-nitrophenol (D, E, F) and 4-nitrophenol (G, H, I).

Table 1 Comparative catalytic performance of MNPs biosynthesized from plant extracts for reduction of nitrophenols by $NaBH_4$.

Nitrophenols	MNPs	Plant extract	Size (nm)	k_{app} ($\times 10^{-3}$, s^{-1})	Ref.
2-NP	AgNPs	*Cassia occidentalis*	10	0.4	Gondwal and Pant, 2018
	AuNPs	Seaweed *Lobophora variegate*	2–12	1.22	Deng et al., 2019
	AgNPs	*Passiflora edulis* peels	25	1.15	This work
	AuNPs		7	1.39	This work
3-NP	AgNPs	*Codonopsis pilosula* root	10	1.71	Doan et al., 2020a
	AgNPs	Corn-cob	11	0.1	Doan et al., 2020c
	AuNPs		35	0.7	
	AgNPs	*Passiflora edulis* peels	25	2.45	This work
	AuNPs		7	0.67	This work
4-NP	AgNPs	*Dodonaea viscosa*	–	1.0	Shah et al., 2021
	AgNPs	*Dimocarpus longan* seed	40	0.47	Khan et al., 2016
	AuNPs	*Sterculia acuminate* fruit	9–38	1.6	Bogireddy et al., 2015
	AuNPs	*Trichosporon montevideense*	12–53	0.52	Shen et al., 2016
	AgNPs	*Passiflora edulis* peels	25	1.58	This work
	AuNPs		7	1.32	This work

Table 2 Comparative catalytic performance of MNPs biosynthesized from plant extracts for reduction of toxic dyes by $NaBH_4$.

Pollutants	MNPs	Plants	Size (nm)	k_{app} (10^{-3}, s^{-1})	Ref.
MO	AgNPs	*Prosopis juliflora*	70–105	2.23	Anwar et al., 2019
	AgNPs	*Dodonaea viscosa*	–	4.8	Shah et al., 2021
	AgNPs	*Zanthoxylum armatum*	15–50	0.03	Jyoti and Singh, 2016
	AuNPs	*Sterculia acuminate* fruit	9–38	0.75	Bogireddy et al., 2015
	AgNPs	*Passiflora edulis* peels	25	5.98	This work
	AuNPs		7	4.26	
EY	AgNPs	*Trigonella foenum-graecum* seed	32	1.3	Vidhu and Philip, 2014
	AgNPs	corn-cob	11	3.8	Doan et al., 2020c
	AuNPs		35	3.9	
	AgNPs	*Passiflora edulis* peels	25	3.35	This work
	AuNPs		7	2.07	
Rh6G	AgNPs	*Cordia obliqua* Willd fruit	7.1	2.57	Saidu et al., 2019
	AuNPs	*Persea americana*	8	3.1	
	AgNPs	*Passiflora edulis* peels	25	3.90	This work
	AuNPs		7	2.36	
RhB	AgNPs	*Dodonaea viscosa*	–	1.3	Shah et al., 2021
	AgNPs	*Crinum latifolium* leaves	20.5	2.91	Vo, et al., 2019
	AuNPs		17.5	3.23	
	AgNPs	*Passiflora edulis* peels	25	8.24	This work
	AuNPs		7	2.63	

4-nitrophenols are found to be 2.27×10^{-9} min^{-1}, 6.25×10^{-9} min^{-1} and 2.50×10^{-9} min^{-1}, respectively while higher values are found for PEP-AuNPs (3.42×10^{-9} min^{-1}, 7.40×10^{-9} min^{-1} and 3.07×10^{-9} min^{-1}, respectively) that is due to lower concentration of gold in PEP-AuNPs used.

Degradation of organic dyes

The catalytic performance of the biogenic nanoparticles was also evaluated in degradation reaction for four toxic organic dyes including MO, EY, Rh6G and RhB. The $NaBH_4$ mediated degradation of these dyes in the absence of the catalyst occurred slowly which can be found elsewhere [T.D. Nguyen et al., 2018]. However, the addition of the synthesized MNPs into the reaction mixture accelerated degradation of the dyes. This could be easily observed from the fading of their color as well as the decrease in the absorbance at relative absorption peaks of MO (464 nm), EY (515 nm), Rh6G (525 nm) and RhB (554 nm). Fig. 12 illustrates the UV–Vis spectra measured during the degradation process using both MNPs and the plots between absorbance values versus reaction time to evaluate their reaction kinetics. The obtained data obviously indicate the catalytic effect of the biosynthesized MNPs significantly dependent on the kind of the organic dyes. The degradation time of the dyes in the presence of PEP-AgNPs is found RhB (6 min), MO (8 min), Rh6G (12 min) and EY (12 min) and the values of rate constant are found to be 8.24×10^{-3} s^{-1}, 5.96×10^{-3} s^{-1}, 3.90×10^{-3} s^{-1} and 3.35×10^{-3} s^{-1}, respectively. Meanwhile, longer catalytic degradation of the respective dyes in the presence of PEP-AuNPs is confirmed with RhB (12 min), MO (12 min), Rh6G (18 min) and EY

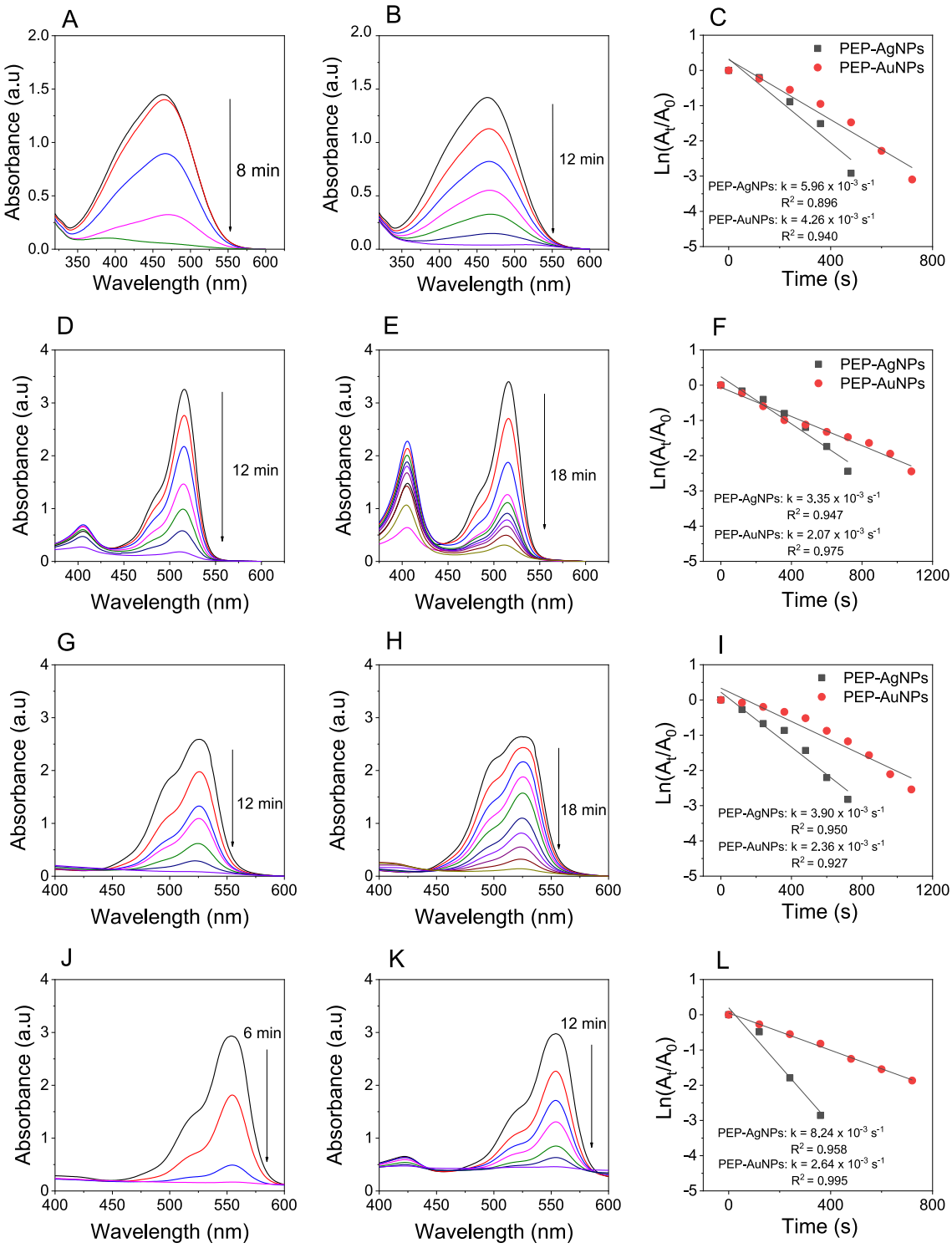

Fig. 12 UV–vis spectra in the presence of PEP-AgNPs (left), UV–vis spectra in the presence of PEP-AuNPs (middle), first order kinetics (right) for degradation of MO (A, B, C), EY (D, E, F), Rh6G (G, H, I) and RhB (J, K, L).

(18 min) and the rate constants are found to be 2.64×10^{-3} s^{-1}, 4.26×10^{-3} s^{-1}, 2.36×10^{-3} s^{-1} and 2.07×10^{-3} s^{-1}, respectively. In general, the catalytic capacity of PEP-AgNPs is significantly higher than the activity of PEP-AuNPs in degradation of these toxic dyes. Our results confirmed the MNPs synthesized from PEP extract as a valuable heterogeneous catalyst for degradation of toxic organic dyes. Additionally, the catalysts synthesized in this work show high performance in comparison with the other researches listed in Table 2. For instant, catalytic activity of PEP-AgNPs in

degradation of MO is 2.7-folds and 200-folds as much as that biosynthesized from *Prosopis juliflora* and *Zanthoxylum armatum* extracts, respectively.

TOF values for catalytic degradation of MO, EY, Rh6G and RhB in the presence of PEP-AgNPs are found to be 6.25×10^{-9} min^{-1}, 4.17×10^{-9} min^{-1}, 4.17×10^{-9} min^{-1} and 8.3×10^{-9} min^{-1}, respectively while slightly higher values for catalysis of PEP-AuNPs are found to be 7.41×10^{-9} min^{-1}, 4.94×10^{-9} min^{-1}, 4.94×10^{-9} min^{-1} and 7.41×10^{-9} min^{-1}, respectively. In general, *Passiflora edulis* fruit peels are an excellently waste material source for production of MNPs that can apply effectively in treatment of industrial wastewater.

4. Conclusions

This study offered a green method for the synthesis of silver and gold nanoparticles and their applications in pharmaceutical and environmental fields. This work utilized successfully waste agricultural source as eco-friendly reducing and stabilizing agents for the fabrication of noble nanoparticles. The crystalline AgNPs and AuNPs were obtained in spherical shape with mean sizes of 25 nm and 7 nm, respectively. AgNPs showed strong antibacterial activity against all tested bacterial strains. MIC values were found to be 0.5 mM for all the strains. The excellent catalysis performance of the nanoparticles has been evaluated for the reduction of nitrophenols and the degradation of four toxic dyes. The waste *P. edulis* fruit peels demonstrated as an excellently agricultural source for green synthesis of noble nanoparticles with potentially multiple applications.

5. Data availability

The data used to support the findings of this study are included within the article.

Declaration of Competing Interest

The authors declare that they have no known competing financial interests or personal relationships that could have appeared to influence the work reported in this paper.

Acknowledgements

This work is supported by Basic Science Research Fund of Tra Vinh University (No. 168/HD.HDKH-DHTV).

Appendix A. Supplementary material

Supplementary data to this article can be found online at https://doi.org/10.1016/j.arabjc.2021.103096.

References

Abdel-Shafy, H.I., Mansour, M.S.M., 2018. Green synthesis of metallic nanoparticles from natural resources and food waste and their environmental application. In: Kanchi, S., Ahmed, S. (Eds.), Green Metal Nanoparticles: Synthesis, Characterization and their Applications, Willy and Scrivener, pp. 321–385.

Ahmad, F., Zhu, D., Sun, J., 2020. Bacterial chemotaxis: a way forward to aromatic compounds biodegradation. Environ. Sci. Eur. 32, 52.

Ali, J., Rasheed, T., Afreen, M., Anwar, M.T., Nawaz, Z., Anwar, H., Rizwan, K., 2020. Modalities for conversion of waste to energy—challenges and perspectives. Sci. Total Environ. 727, 138610.

Anwar, Y., Fakieh, M.H., Ullah, I., Alkenani, N.A., Sharif, M.A., 2019. Synthesis of silver nanoparticles using Prosopis juliflora extract: potential of antimicrobial and pollutants degradation performance. Desalin. Water Treat. 167, 105.

Astruc, D., 2020. Introduction: nanoparticles in catalysis. Chem. Rev. 120, 461–463.

Bogireddy, N.K.R., An, K.K.H., Mandal, B.K., 2015. Gold nanoparticles—synthesis by Sterculia acuminata extract and its catalytic efficiency in alleviating different organic dyes. J. Mol. Liq. 211, 868.

Capasso, C., Supuran, C.T., 2014. Sulfa and trimethoprim-like drugs – antimetabolites acting as carbonic anhydrase, dihydropteroate synthase and dihydrofolate reductase inhibitors. J. Enzyme Inhib. Med. Chem. 29, 379.

Chen, J., Lü, S., Zhang, Z., Zhao, X., Li, X., Ning, P., Liu, M., 2018. Environmentally friendly fertilizers: a review of materials used and their effects on the environment. Sci. Total Environ. 613–614, 829.

Cíntia, B.L., Fávaro-Polonio, Z., Julio, J.A.P., Polonio, C., 2019. Effects of textile dyes on health and the environment and bioremediation potential of living organisms. Biotechnol. Res. Innov. 3, 275.

Clissold, S.P., 1986. Paracetamol and phenacetin. Drugs 32, 46.

Deng, X., Fu, Y., Luo, Luo, S.X., Wang, Q., Hu, M., Ma, F., Ma, C. W., Zhou, L., 2019. Polysaccharide from Radix Codonopsis has beneficial effects on the maintenance of T-cell balance in mice. Biomed. Pharmacother. 112.

Doan, V.D., Huynh, B.A., Nguyen, T.D., Cao, X.T., Nguyen, V.C., Nguyen, T.L.H., Nguyen, H.T., Le, V.T., 2020a. Biosynthesis of silver and gold nanoparticles using aqueous extract of *Codonopsis pilosula* roots for antibacterial and catalytic applications. J. Nanomater. 2020, 8492016.

Doan, V.D., Phung, M.T., Nguyen, T.L.H., Mai, T.C., Nguyen, T.D., 2020b. Noble metallic nanoparticles from waste *Nypa fruticans* fruit husk: biosynthesis, characterization, antibacterial activity and recyclable catalysis. Arab. J. Chem. 13, 7490.

Doan, V.D., Luc, V.S., Nguyen, T.L.H., Nguyen, T.D., Nguyen, T.D., 2020c. Utilizing waste corn-cob in biosynthesis of noble metallic nanoparticles for antibacterial effect and catalytic degradation of contaminants. Environ. Sci. Pollut. Res. 27, 6148.

Gondwal, M., Pant, G.J., 2018. Synthesis and Catalytic and Biological Activities of Silver and Copper Nanoparticles Using *Cassia occidentalis*. Int. J. Biomater. 2018, 6735426.

Goss, M.J., Nunes, M.L.O., Machado, I.D., Merlin, L., Macedo, N. B., Silva, A.M.O., Bresolin, T.M.B., Santin, J.R., 2018. Peel flour of *Passiflora edulis* Var. Flavicarpa supplementation prevents the insulin resistance and hepatic steatosis induced by low-fructose-diet in young rats. Biomed. Pharmacother. 102, 848.

Ismail, M., Akhtar, K., Khan, M.I., Kamal, T., Khan, M.A., Asiri, A. M., Seo, J., Khan, S.B., 2019. Pollution, toxicity and carcinogenicity of organic dyes and their catalytic bio-remediation. Curr. Pharm. Des. 25, 3645.

Jain, S., Hirst, D.G., O'Sullivan, J.M., 2012. Gold nanoparticles as novel agents for cancer therapy. Br. J. Radiol. 85, 101.

Jain, S., Mehata, M.S., 2017. Medicinal plant leaf extract and pure flavonoid mediated green synthesis of silver nanoparticles and their enhanced antibacterial property. Sci. Rep. 7, 15867.

Jeevanandam, J., Barhoum, A., Chan, Y.S., Dufresne, A., Danquah, M.K., 2018. Review on nanoparticles and nanostructured materials: history, sources, toxicity and regulations. Beilstein J. Nanotechnol. 9, 1050.

Jyoti, K., Singh, A., 2016. Green synthesis of nanostructured silver particles and their catalytic application in dye degradation. J. Genet. Eng. Biotechnol. 14, 311.

Keijok, W.J., Pereira, R.H.A., Alvarez, L.A.C., Prado, A.R., da Silva, A.R., Ribeiro, J., de Oliveira, J.P., Guimarães, M.C.C., 2019. Controlled biosynthesis of gold nanoparticles with *Coffea arabica* using factorial design. Sci. Rep. 9, 16019.

Khameneh, B., Iranshahy, M., Soheili, V., Bazzaz, B.S.F., 2019. Review on plant antimicrobials: a mechanistic viewpoint. Antimicrob. Resist Infect. Control. 8, 118.

Khan, I., Saeed, K., Khan, I., 2019. Nanoparticles: properties, applications and toxicities. Arab. J. Chem. 12, 908.

Khan, F.U., Chen, Y., Khan, N.U., Khan, Z.U.H., Khan, A.U., Ahmad, A., Tahir, K., Wang, L., Khan, M.R., Wan, P., 2016. Antioxidant and catalytic applications of silver nanoparticles using *Dimocarpus longan* seed extract as a reducing and stabilizing agent. J. Photochem. Photobiol. B 164, 344.

Lanzafame, P., Perathoner, S., Centi, G., Gross, S., Hensen, E.J.M., 2017. Grand challenges for catalysis in the Science and Technology Roadmap on Catalysis for Europe: moving ahead for a sustainable future. Catal. Sci. Technol. 7, 5182.

Lide, D.R., ed., 2006. CRC Handbook of Chemistry and Physics, 87th ed. Boca Raton, FL: CRC Press. 2608 pp.

Maldonado-Muñiz, M., Luna, C., Mendoza-Reséndez, R., Barriga-Castro, E.D., Soto-Rodriguez, S., Ricque-Marie, D., Cruz-Suarez, L.E., 2020. Silver nanoparticles against acute hepatopancreatic necrosis disease (AHPND) in shrimp and their depuration kinetics. J. Appl. Phycol. 32, 2431.

Mitsudome, T., Kaneda, K., 2013. Gold nanoparticle catalysts for selective hydrogenations. Green Chem. 15, 2636.

Ncube, L.K., Ude, A.U., Ogunmuyiwa, E.N., Zulkifli, R., Beas, I.N., 2020. Environmental impact of food packaging materials: a review of contemporary development from conventional plastics to polylactic acid based materials. Materials 13, 4994.

Nguyen, T.D., Dang, C.H., Mai, D.T., 2018a. Biosynthesized AgNP capped on novel nanocomposite 2-hydroxypropyl-β-cyclodextrin/alginate as a catalyst for degradation of pollutants. Carbohydr. Polym. 197, 29.

Nguyen, T.T.N., Vo, T.T., Nguyen, B.N.H., Nguyen, D.T., Dang, V.S., Dang, C.H., Nguyen, T.D., 2018b. Silver and gold nanoparticles biosynthesized by aqueous extract of burdock root, *Arctium Lappa* as antimicrobial agent and catalyst for degradation of pollutants. Environ. Sci. Pollut. Res. 25, 34247.

Priyadarshini, E., Pradhan, N., 2017. Gold nanoparticles as efficient sensors in colorimetric detection of toxic metal ions: a review. Sens. Actuators B Chem. 238, 888.

Rajeshkumar, S., 2016. Anticancer activity of eco-friendly gold nanoparticles against lung and liver cancer cells. J. Genet. Eng. Biotechnol. 14, 195.

Sabela, M., Balme, S., Bechelany, M., Janot, J.M., Bisetty, K., 2017. A review of gold and silver nanoparticle-based colorimetric sensing assays. Adv. Eng. Mater. 19, 1700270.

Saidu, F.K., Mathew, A., Parveen, A., Valiyathra, V., Thomas, G.V., 2019. Novel green synthesis of silver nanoparticles using clammy cherry (*Cordia obliqua* Willd) fruit extract and investigation on its catalytic and antimicrobial properties. SN Appl. Sci. 1, 1368.

Samyn, P., Barhoum, A., Öhlund, T., Dufresne, A., 2018. Review: nanoparticles and nanostructured materials in papermaking. J. Mater. Sci. 53, 146.

Seixas, F.L., Fukuda, D.L., Turbiani, F.R.B., Garcia, P.S., Petkowicz, C.L. de O., Jagadevan, S., Gimenes, M.L. 2014. Extraction of pectin from passion fruit peel (Passiflora edulis f. flavicarpa) by microwave-induced heating. Food Hydrocoll. 38, 186.**

Shah, Z., Gul, T., Khan, S.A., Shaheen, K., Anwar, Y., Suo, H., Ismail, M., Alghamdi, K.M., Salman, S.M., 2021. Synthesis of high surface area AgNPs from Dodonaea viscosa plant for the removal of pathogenic microbes and persistent organic pollutants. Mater. Sci. Eng. B 263, 114770.

Shankar, P.D., Shobana, S., Karuppusamy, I., Pugazhendhi, A., Ramkumar, V.S., Arvindnarayan, S., Kumar, G., 2016. A review on the biosynthesis of metallic nanoparticles (gold and silver) using bio-components of microalgae: Formation mechanism and applications. Enzyme Microb. Technol. 95, 28.

Shen, W., Qu, Y., Pei, X., Zhang, X., Ma, Q., Zhang, Z., Li, S., Zhou, J., 2016. Green synthesis of gold nanoparticles by a newly isolated strain *Trichosporon montevideense* for catalytic hydrogenation of nitroaromatics. Biotechnol. Lett. 38, 1503.

Singh, D., Singh, S., Sahu, J., Srivastava, S., Singh, M.R., 2016a. Ceramic nanoparticles: Recompense, cellular uptake and toxicity concerns. Artif. Cells Nanomed. Biotechnol. 44, 401.

Singh, P., Kim, Y.J., Yang, D.C., 2016b. A strategic approach for rapid synthesis of gold and silver nanoparticles by *Panax ginseng* leaves. Artif. Cells Nanomed. Biotechnol. 44, 1949.

Talapko, J., Matijevic, T., Juzbasic, M., Antolovic-Pozgain, A., Skrlec, I., 2020. Antibacterial Activity of Silver and Its Application in Dentistry. Cardiology and Dermatology. Microorganisms 8, 1400.

Tang, S., Zheng, J., 2018. Antibacterial Activity of Silver Nanoparticles: Structural Effects. Advanced Healthcare Materials. Adv. Healthcare Mater. 2018, 1701503.

Vidhu, V.K., Philip, D., 2014. Catalytic degradation of organic dyes using biosynthesized silver nanoparticles. Micron 56, 54–62.

Vo, T.T., Nguyen, T.T.N., Huynh, T.T.T., Vo, T.T.T., Nguyen, T.T.N., Nguyen, D.T., Dang, V.S., Dang, C.H., Nguyen, T.D., 2019. Biosynthesis of silver and gold nanoparticles using aqueous extract of *Crinum latifolium* leaf and their applications towards antibacterial effect and wastewater treatment. J Nanomater. 2019, 8385935.

Vuolo, M.M., Cariello Lima, G., Junior, M.R.M. 2019. Passiflora edulis Peel Flour and Health Effects, in Flour and Breads and their Fortification in Health and Disease Prevention (2nd Edition), Ed. V. R. Preedy and R. R. Watson, Academic Press, 249-258.

Yadi, M., Mostafavi, E., Saleh, B., Davaran, S., Aliyeva, I., Khalilov, R., Nikzamir, M., Nikzamir, N., Akbarzadeh, A., Panahi, Y., Milani, M., 2018. Current developments in green synthesis of metallic nanoparticles using plant extracts: a review. Artif. Cells Nanomed. Biotechnol. 46, S336.

Zeng, E.Y., You, J., Cheng, H., 2011. Balance between economic growth and environmental protection: sustainability through better science. J. Environ. Monit. 13, 787.

Zielinska, A., Carreiro, F., Oliveira, A.M., Neves, A., Pires, B., Venkatesh, D.N., Durazzo, A., Lucarini, M., Eder, P., Silva, A.M., Santini, A., Souto, E.B., 2020. Polymeric Nanoparticles: Production, Characterization. Toxicology and Ecotoxicology. Molecules 25, 3731.